

Multi-goal Rapidly Exploring Random Tree with Safety and Dynamic Constraints for UAV Cooperative Path Planning

Thu Hang Khuat^{1*} , Duy-Nam Bui¹ , Hoa TT. Nguyen²,
Mien L. Trinh³ , Minh T. Nguyen² , Manh Duong Phung⁴  *Senior Member, IEEE*

Abstract—Cooperative path planning is gaining its importance due to the increasing demand on using multiple unmanned aerial vehicles (UAVs) for complex missions. This work addresses the problem by introducing a new algorithm named MultiRRT that extends the rapidly exploring random tree (RRT) to generate paths for a group of UAVs to reach multiple goal locations at the same time. We first derive the dynamics constraint of the UAV and include it in the problem formulation. MultiRRT is then developed, taking into account the cooperative requirements and safe constraints during its path-searching process. The algorithm features two new mechanisms, node reduction and Bezier interpolation, to ensure the feasibility and optimality of the paths generated. Importantly, the interpolated paths are proven to meet the safety and dynamics constraints imposed by obstacles and the UAVs. A number of simulations, comparisons, and experiments have been conducted to evaluate the performance of the proposed approach. The results show that MultiRRT can generate collision-free paths for multiple UAVs to reach their goals with better scores in path length and smoothness metrics than state-of-the-art RRT variants including Theta-RRT, FN-RRT, RRT*, and RRT*-Smart. The generated paths are also tested in practical flights with real UAVs to evaluate their validity for cooperative tasks. The source code of the algorithm is available at https://github.com/duynamrcv/multi-target_RRT

Index Terms—Cooperative path planning, rapidly exploring random tree, unmanned aerial vehicle

I. INTRODUCTION

In recent years, the use of multiple unmanned aerial vehicles (UAVs) has emerged as an essential approach for tackling increasingly complex and demanding tasks. By distributing resources and combining sensor data, multiple UAVs can achieve expanded operational areas, faster data collection, and increased mission robustness [1]–[4]. These capabilities are particularly advantageous in many applications such as search

and rescue operations, environmental monitoring, disaster response, and precision agriculture, where extensive coverage and real-time data collection from multiple perspectives are important. To obtain these capabilities, the UAVs need a robust and effective cooperative path planning system to guide them through complex environments, avoid collisions, and optimize their routes.

In cooperative path planning, the goal is to find a feasible path for each UAV from its start to its final location, fulfilling several requirements and constraints [5], [6]. The requirements involve task allocation and optimality, such as arriving at certain locations at the same time, minimizing the path length and energy consumption, and maintaining communication [7]–[10]. The constraints relate to UAV dynamics and safety such as turning angles and distance to obstacles. Approaches to this problem can be categorized into four primary groups including mathematical programming, swarm intelligence, artificial potential field, and graph-based planning methods.

Mathematical programming addresses the path planning problem by modeling it as an optimization where the aim is to minimize or maximize an objective function subject to a set of constraints. Programming techniques such as mixed integer programming (MIP), nonlinear programming (NP), and dynamic programming (DP) are then used to solve the problem [11]–[13]. In [11], the coverage path planning problem for multiple robots is reduced to the min-max rooted tree cover problem. An MIP model is then proposed to solve that problem to find the paths. In [14], a set of mixed integer linear programming models is introduced to find the paths for multiple robots to capture a moving target within a given time limit. In [15], a neuro-dynamic programming algorithm is proposed to generate paths that allow the UAVs to avoid threat zones and arrive at the targets at the same time from different directions. These approaches provide suboptimal solutions and offer flexibility to handle multiple constraints. However, their performance depends on the definition of objective functions, which are often simplified representations of the real-world scenario. In addition, the computational cost of mathematical programming techniques grows exponentially as the scale of the planning problem increases.

Similar to mathematical programming, swarm intelligence techniques also formulate path planning as an optimization problem. However, they use nature-inspired algorithms such as the genetic algorithm (GA) and particle swarm optimization

*Corresponding author

¹Thu Hang Khuat and Duy-Nam Bui are with the Vietnam National University, Hanoi, Vietnam. 23025115@vnu.edu.vn; duynam@ieee.org

²Hoa TT. Nguyen and Minh T. Nguyen are with the Thai Nguyen University of Technology, Thai Nguyen University, Thai Nguyen, Vietnam. nguyenthituyethoa@tnut.edu.vn; nguyentuanminh@tnut.edu.vn

³Mien L. Trinh is with the University of Transport and Communications, Hanoi, Vietnam. mientl@utc.edu.vn

⁴Manh Duong Phung is with the Fulbright University Vietnam, Ho Chi Minh City, Vietnam. duong.phung@fulbright.edu.vn

The authors would like to thank the Master, PhD Scholarship Programme (Code: VINIF.2023.Ths.044) of Vingroup Innovation Foundation (VINIF) and the Ministry of Education and Training (Project B2023-GHA-01), Viet Nam, for the support on this work.

(PSO) to solve it. These techniques utilize swarm intelligence, such as social and collective behaviors, to better explore and exploit the search space for the optimal solutions. In [16], the GA is used to solve the cooperative reconnaissance path planning for multiple UAVs taking off from different bases. In [17], maximum-minimum ant colony optimization and differential evolution are combined to generate collision-free paths for multiple UAVs. An improved grey wolf optimizer is introduced in [18] to solve the trajectory planning subject to various constraints. Other algorithms such as PSO and ant colony optimization (ACO) are also used in [6], [19], [20] to address the cooperative path planning problem with different constraints and requirements. The main advantages of nature-inspired algorithms lie in their simple structure and fast generation of solutions [18]. The quality of the solutions, however, depends on the initialization, population size, and mechanism to avoid local optimum.

Artificial potential field (APF) is another approach that addresses the path planning problem by simulating virtual forces that influence the UAV [21], [22]. In this method, the goal generates attractive forces while obstacles create repulsive forces so that they together drive the robot through the environment like a particle moving in a force field. In particular, a rotating potential field is used in [23] to generate paths for a multi-UAV system that can avoid local minimum. In [24], an improved APF is introduced where the k-means algorithm is used to optimize attractive forces. The paths generated by APF, however, are not optimal since they do not include a cost function for evaluation. Local optimum is also another issue as the attractive and repulsive forces can be equal at certain potential points [22].

Graph-based path planning is another direction that represents the environment as a network of nodes and edges, where nodes represent possible positions and edges represent viable paths between them [25]. This representation allows algorithms such as probabilistic roadmap (PRM) [26] and rapidly-exploring random tree (RRT) [27] to determine the route from a starting point to a destination. In [28], the PRM is used to generate paths for UAVs in complex 3D environments in which the A* is utilized to find feasible paths. In [29], the RRT is employed to generate flyable paths in real time for UAVs. While the graph-based approach is fast and efficient, the paths generated are not optimized due to its random expansion mechanism. Some improvements have been introduced to address this issue such as RRT* [30] and RRT*-Smart [31]. They however do not consider safety and dynamic constraints which are critical to generate feasible paths for UAVs.

Recently, deep reinforcement learning has been used to model environmental dynamics and optimize UAV trajectories [32]. For instance, a deep Q network is introduced in [33] to control the movements of the UAVs in adaption to the terrestrial structure for Peer-to-Peer (P2P) communication between UAVs. However, this method requires significant computational resources for both training and real-time decision-making and faces difficulties in generalizing learned policies across different environments with multiple moving UAVs. In addition, multiple UAVs also bring new challenges

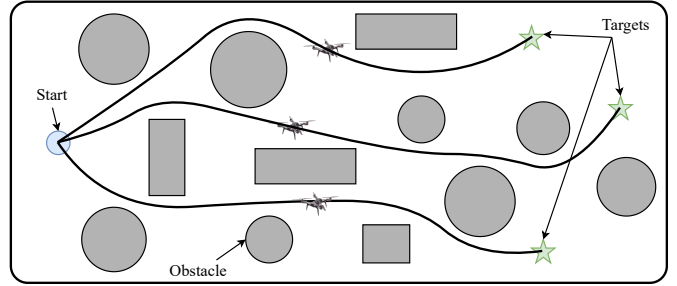


Fig. 1: A cooperative path planning task where multiple UAVs need to reach different target locations at the same time

related to their heterogeneous capability, task allocation, and time coordination. The high mobility of UAVs causes the topology of multi-UAVs to become dynamic, which makes the UAVs' communication connections sparse and intermittent [34], [35]. Therefore, incorporating time coordination, dynamic constraints, and path smoothing into path planning to increase its feasibility and efficiency is a problem that is worth further investigation.

In this work, we address the cooperative path planning problem by introducing a new algorithm, named MultiRRT, to generate paths for multiple UAVs cooperated in a complex environment. We first formulate the problem by defining the task requirements, UAV models, and dynamics constraints. MultiRRT is then introduced to solve the problem by generating paths for multiple UAVs. Several new mechanisms have been included in the algorithm to optimize the paths. Our contributions are threefold:

- i. Derivation of the dynamic constraint of the quadrotor UAV, which is essential to generate flyable paths.
- ii. Proposal of MultiRRT that incorporates safety and dynamics constraints during its branch expansion to find paths to multiple goal locations. The algorithm also features a new node reduction mechanism to optimize the path length.
- iii. Introduction of a new Bezier interpolation technique to smooth the flight paths. The interpolated paths are proven to be collision-free and satisfy the dynamic constraint.

The rest of this paper is organized as follows. Section II describes the cooperative path planning problem. Section III introduces the UAV model and the calculation of its dynamic constraint. Section IV presents the proposed path planning algorithm for multiple UAVs. Simulations, comparisons, and experiments are presented in Section V. The paper ends with a conclusion drawn in Section VI.

II. PROBLEM FORMULATION

This study considers a group of UAVs that must traverse a complex environment to reach different target locations and complete tasks such as disaster rescue or emergency network establishment, as shown in Figure 1. Assuming that there are n target locations, the task involves finding n paths that meet the following requirements:

- i. Guide the UAVs to simultaneously arrive n pre-defined locations;

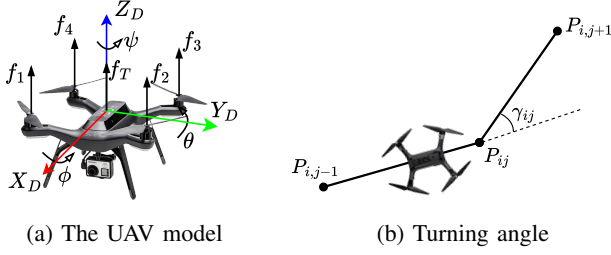


Fig. 2: UAV model and its turning angle

- ii. Satisfy constraints imposed by the UAV's dynamics;
- iii. Ensure that there are no collisions among the UAVs or between the UAVs and their operating environment.

The first requirement allows the UAVs to fulfill their cooperative task, while the second and third ones maintain their safety and efficiency. In our approach, the UAVs are modeled like Dubins vehicles flying at a fixed altitude with a constant forward speed, a widely adopted model for UAVs [36]–[38]. In this model, the collision among UAVs can be avoided by simply choosing a different flight altitude for each UAV, i.e., $h_i \neq h_q, \forall i \neq q \in \{1, \dots, n\}$, where h_i is the altitude of UAV i . Let v_i be the speed of UAV i and L_i be the length of path \mathcal{P}_i . The cooperation in time among the UAVs then can be obtained by choosing v_i so that it is inversely proportional to the path length, i.e.,

$$\frac{L_i}{v_i} = \frac{L_{i+1}}{v_{i+1}} \quad \forall i = 1, \dots, n-1. \quad (1)$$

To include dynamic constraints, this work presents path \mathcal{P}_i as a set of N_i line segments consisting of $N_i + 1$ points P_{ij} . A flyable path then needs to have its turning angles staying within the maneuverable limits of the UAV. Let γ_{ij} be the turning angle at P_{ij} , which is defined by the angle between two vectors $\overrightarrow{P_{i,j-1}P_{ij}}$ and $\overrightarrow{P_{ij}P_{i,j+1}}$, as illustrated in Figure 2b. It is given by

$$\gamma_{ij} = \cos^{-1} \left(\frac{\overrightarrow{P_{i,j-1}P_{ij}} \cdot \overrightarrow{P_{ij}P_{i,j+1}}}{\|\overrightarrow{P_{i,j-1}P_{ij}}\| \|\overrightarrow{P_{ij}P_{i,j+1}}\|} \right). \quad (2)$$

Denote γ_{\max} as the maximum turning angle of the UAV. A flyable path then needs to meet the following condition:

$$\gamma_{ij} \leq \gamma_{\max}, \quad \forall j \in \{2, \dots, N\}. \quad (3)$$

The value of γ_{\max} can be computed based on the UAV dynamics presented in the next section.

III. UAV DYNAMIC MODEL AND CONSTRAINT ANALYSIS

A. Dynamic model

The UAVs used in this work are quadcopters with two pairs of propellers rotating in opposite directions, as depicted in Figure 2a. Let $f_l, l = \{1, 2, 3, 4\}$, be the thrust generated by propeller l . According to [39], f_l is proportional to the square of rotational speed Ω_l of motor l , i.e.,

$$f_l = c_t \Omega_l^2 \quad \forall l = 1, 2, 3, 4, \quad (4)$$

where c_t is the thrust coefficient. The total thrust is then given by

$$f_T = \sum_{k=1}^4 f_l. \quad (5)$$

Since f_T acts along the Z_D axis, the thrust vector in the body frame is given by $f_D = [0, 0, f_T]^T$. Apart from the thrust, the UAV is also influenced by drag force, f_d , caused by air friction. It is proportional to the UAV's linear velocities, i.e., $f_d = c_f [\dot{x}, \dot{y}, \dot{z}]^T$, where c_f is the friction coefficient. The motion of the UAV in the inertial frame is then driven by the gravitational, thrust, and drag forces. Let R be the rotation matrix mapping the body frame to the inertial frame, then

$$R_{xyz} = R_z(\psi) R_y(\theta) R_x(\phi) \quad (6)$$

with

$$R_z(\psi) = \begin{bmatrix} \cos \psi & -\sin \psi & 0 \\ \sin \psi & \cos \psi & 0 \\ 0 & 0 & 1 \end{bmatrix}$$

$$R_y(\theta) = \begin{bmatrix} \cos \theta & 0 & \sin \theta \\ 0 & 1 & 0 \\ -\sin \theta & 0 & \cos \theta \end{bmatrix} \quad (7)$$

$$R_x(\phi) = \begin{bmatrix} 1 & 0 & 0 \\ 0 & \cos \phi & -\sin \phi \\ 0 & \sin \phi & \cos \phi \end{bmatrix}$$

where ϕ, θ , and ψ are respectively the roll, pitch, and yaw angles, and R_x, R_y , and R_z are respectively the rotation matrices about the x, y , and z axes. The dynamic equations describing the linear motion of the UAV are then given by

$$\begin{bmatrix} \ddot{x} \\ \ddot{y} \\ \ddot{z} \end{bmatrix} = \frac{1}{m} \left(R_{xyz} f_D - f_d - \begin{bmatrix} 0 \\ 0 \\ mg \end{bmatrix} \right), \quad (8)$$

where m is the mass of the UAV and g is the gravitational acceleration.

B. Dynamic constraint analysis

Assume that at time t , the UAV is flying along X_D at velocity v_x with pitching angle θ . The UAV then tries to turn an angle γ_{\max} in direction Y_D by carrying out a rotation of an angle ϕ about the X_D axis. The calculation of γ_{\max} then can be derived as follows.

Let $f_I = [f_{Ix}, f_{Iy}, f_{Iz}]^T$ be the force acting on the UAV in the inertial frame. This force relates to f_D by the rotations of ϕ and θ about the X_D and Y_D axes as follows:

$$f_I = R_y(\theta) R_x(\phi) f_D = \begin{bmatrix} f_T \cos \phi \sin \theta \\ -f_T \sin \phi \\ f_T \cos \phi \cos \theta \end{bmatrix}. \quad (9)$$

Since the UAV flies at constant speed v_x , thrust force f_{I_x} is balanced with drag force f_{dx} . From (9), we get

$$f_{I_x} = f_T \cos \phi \sin \theta = c_f v_x. \quad (10)$$

When the UAV turns, f_{I_y} will generate centripetal acceleration, a_y , in Y_B direction and v_x will become the tangential velocity, i.e.,

$$f_{I_y} = -ma_y = -\frac{mv_x^2}{R}, \quad (11)$$

where R is the turning radius and the negative sign implies that the direction of a_y is opposite of the Y_B axis. Substituting f_{I_y} from (9) to (11) gives

$$f_T \sin \phi = \frac{mv_x^2}{R}. \quad (12)$$

As the UAV flies at a fixed altitude, the force f_{I_z} acting in z direction is balanced with the gravity. We have

$$f_{I_z} = f_T \cos \phi \cos \theta = mg. \quad (13)$$

From (10) and (13), pitch angle θ can be computed as follows:

$$\theta = \tan^{-1} \left(\frac{c_f v_x}{mg} \right). \quad (14)$$

Substituting (14) into (13) gives

$$\phi = \cos^{-1} \left(\frac{c_f v_x}{f_T \sin \theta} \right). \quad (15)$$

On the other hand, from (14), we get

$$\sin \theta = \frac{1}{\sqrt{\frac{1}{\tan^2 \theta} + 1}} = \frac{c_f v_x}{\sqrt{c_f^2 v_x^2 + m^2 g^2}}. \quad (16)$$

Rearranging (12) and substituting (15) and (16) into it give

$$R = \frac{mv_x^2}{f_T \sqrt{1 - \cos^2 \phi}} = \frac{mv_x^2}{\sqrt{f_T^2 - c_f^2 v_x^2 - m^2 g^2}}. \quad (17)$$

As the turning angle γ is inversely proportional to the turning radius R and v_x is constant, we have

$$\gamma_{\max} = \frac{1}{R_{\min}} = \frac{\sqrt{f_{T\max}^2 - c_f^2 v_x^2 - m^2 g^2}}{mv_x^2}, \quad (18)$$

where $f_{T\max}$ is the maximum thrust force. The maximum turning angle γ_{\max} defines the limit at which a controller can adjust the UAV's direction to follow the planned path. The path planning algorithm therefore must take into account this constraint when generating paths to ensure they are feasible for the UAV to follow in practice.

IV. MULTIRRT FOR COOPERATIVE PATH PLANNING

This section presents our approach to address the cooperative path planning problem by extending the RRT for multiple goals.

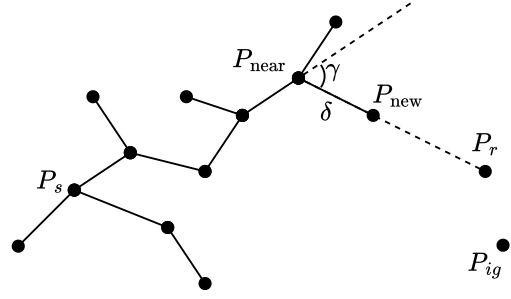


Fig. 3: Illustration of the enhanced RRT algorithm with the constraint on the turning angle

A. Multi-goal RRT with dynamic constraint

Denote P_s as the start location of the UAVs and P_{ig} as the goal location for UAV i . The path for the i^{th} UAV is represented by a set of nodes $\mathcal{P}_i = \{P_{ij}\}, \forall j \in \{1, \dots, N_i + 1\}$. Denote \mathcal{G} as the RRT tree that contains all paths \mathcal{P}_i , i.e., $\mathcal{P}_i \subset \mathcal{G}, \forall i \in \{1, \dots, n\}$. \mathcal{G} is formed through an expansion process that involves random nodes. The expansion starts with a node P_r chosen randomly within the environment, as illustrated in Figure 3. Let $P_{\text{near}} \in \mathcal{G}$ be the node closest to P_r . A new node P_{new} is then created to lie on the vector $\overrightarrow{P_{\text{near}}P_r}$ with a predefined distance δ as follows

$$\left\{ \begin{array}{l} \overrightarrow{P_{\text{near}}P_r} = \lambda \overrightarrow{P_{\text{near}}P_{\text{new}}} \\ \left\| \overrightarrow{P_{\text{near}}P_{\text{new}}} \right\| = \min \left\{ \left\| \overrightarrow{P_{\text{near}}P_r} \right\|, \delta \right\}, \end{array} \right. \quad (19)$$

where $\lambda \neq 0$ is a scalar. In our work, P_{new} is only added to tree \mathcal{G} if it satisfies two conditions: (i) the line segment connecting this node to its nearest neighbor (P_{near}) is collision-free; and (ii) the turning angle of the resulting path segment does not exceed the maximum turning angle (γ_{\max}). The first condition guarantees safety while the second ensures that the generated paths meet the UAVs' dynamic constraints. In collision checking, the UAV's size is considered by expanding the boundaries of obstacles in the environment by an amount equal to the UAV's radius. For the turning angle, assume P_{new} is connected to node $P_k \in \mathcal{G}$ and P_{k-1} is the parent node of P_k . The turning angle γ at P_k is then the angle between $\overrightarrow{P_{k-1}P_k}$ and $\overrightarrow{P_kP_{\text{new}}}$. This angle needs to meet constraint (3) for P_{new} to be added to \mathcal{G} , i.e.,

$$\gamma = \cos^{-1} \left(\frac{\overrightarrow{P_{k-1}P_k} \cdot \overrightarrow{P_kP_{\text{new}}}}{\left\| \overrightarrow{P_{k-1}P_k} \right\| \left\| \overrightarrow{P_kP_{\text{new}}} \right\|} \right) \leq \gamma_{\max}. \quad (20)$$

Algorithm 1 presents implementation of the algorithm, where the tree expansion only stops if all goal locations P_{ig} are added to the tree. The paths to all goals are then generated by tracing back the tree.

B. Node reduction mechanism

The paths generated by RRT are not optimal due to its random expansion fashion. We address this using a node reduction algorithm as illustrated in Figure 4. First, the algorithm checks if there exists a node P_{ij} nearby the start node P_s and a

Algorithm 1: Pseudo code of the enhanced RRT algorithm with dynamic constraint

```

/* Initialization */
1  $\mathcal{P}_i \leftarrow \emptyset, \forall i \in \{1, \dots, n\};$ 
2  $\mathcal{G} \leftarrow P_s;$ 
3 count  $\leftarrow 0;$  /* number of paths */
/* Path generation via tree expansion */
4 while count  $\neq n$  do
5   Generate random node  $P_r;$ 
6   Find node  $P_{\text{near}} \in \mathcal{G}$  nearest to  $P_r;$ 
7   Generate node  $P_{\text{new}}$  based on equation (19);
8   if  $\overrightarrow{P_{\text{near}}P_{\text{new}}}$  is collision-free and satisfies constraint (20) then
9      $\mathcal{G} \leftarrow P_{\text{new}};$ 
10    for  $i \leftarrow 1$  to  $n$  do
11      if  $\overrightarrow{P_{\text{new}}P_{i_g}}$  is collision-free and satisfies constraint (20) then
12         $\mathcal{G} \leftarrow P_{i_g};$ 
13        Generate path  $\mathcal{P}_i$  by tracing back tree  $\mathcal{G}$  from end node  $P_{i_g};$ 
14        count  $\leftarrow$  count + 1;

```

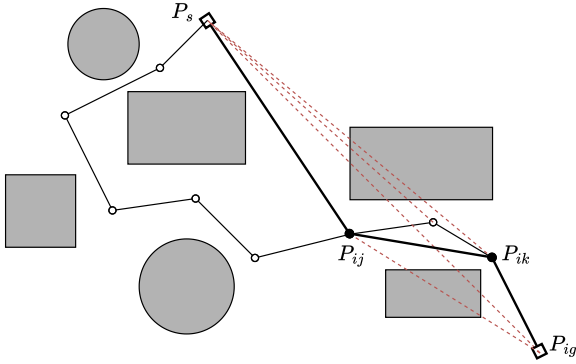


Fig. 4: Illustration of redundant node reduction using the triangle inequality

node P_{ik} nearby the goal P_{ig} . It then evaluates if the path segment $P_{ij}P_{ik}$ is collision-free and satisfies constraint (20). The algorithm finally connects P_{ij} to P_{ik} and removes the nodes between them to form a shorter path. Denote $P_{i,\text{tail}}$ as the end node of \mathcal{P}_i , the node reduction algorithm is presented in Algorithm 2.

C. Path smoothing using Bezier curves

The paths generated by RRT include a set of interconnected line segments that need to be smoothed for the UAVs to follow. We conduct this using an interpolation technique in which a Bezier curve is fitted to each node of the flight path. First, a safe zone is defined at each node as follows.

Definition 1. A safe zone is a circular area around a node whose radius is the distance from that node to its nearest

Algorithm 2: Pseudo code of the node reduction mechanism

```

/* Initialization */
1 Create a copy path  $\mathcal{P}'_i \leftarrow \mathcal{P}_i;$ 
2 Reset  $\mathcal{P}_i \leftarrow \emptyset$  then  $\mathcal{P}_i \leftarrow \mathcal{P}'_i;$ 
/* Remove redundant nodes */
3 while  $P_{i,\text{tail}} \neq P_{i_g}$  do
4   foreach  $P_{ij} \in \mathcal{P}'_i$  do
5     if  $\overrightarrow{P_{i,\text{tail}}P_{ij}}$  is collision-free and satisfy constraint (20) then
6        $\mathcal{P}_i \leftarrow P_{ij};$ 
7       break;
8     end
9   end
10 end

```

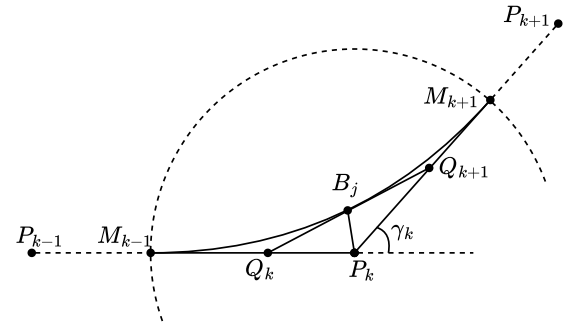


Fig. 5: The safe zone and its intersection with path segments

obstacle.

Consider the safe zone at node P_k with radius R_k that intersects path segments $P_{k-1}P_k$ and P_kP_{k+1} at M_{k-1} and M_{k+1} , respectively, as depicted in Figure 5. Denote $M_k \equiv P_k$, the two first-order curves $H_1(\tau)$ and $H_2(\tau)$ can be created from M_{k-1} , M_k , and M_{k+1} as follows

$$\begin{aligned}
 H_1(\tau) &= M_{k-1} + \tau(M_k - M_{k-1}) \quad 0 \leq \tau \leq 1 \\
 H_2(\tau) &= M_k + \tau(M_{k+1} - M_k) \quad 0 \leq \tau \leq 1.
 \end{aligned} \tag{21}$$

The quadratic Bezier curve $B_k(\tau)$ is then created from $H_1(\tau)$ and $H_2(\tau)$ as

$$\begin{aligned}
 B_k(\tau) &= \tau H_1(\tau) + (1 - \tau)H_2(\tau) \\
 &= (1 - \tau)^2 M_{k-1} + 2(1 - \tau)\tau M_k + \tau^2 M_{k+1}.
 \end{aligned} \tag{22}$$

Theorem 1. The second order Bezier curve $B_k(\tau)$ defined in (22) always lies within the safe zone at point P_k . That is, the distance from any point B_j on $B_k(\tau)$ to P_k is always less than or equal to the radius of the safe zone at P_k :

$$\|P_k B_j\| \leq R_k \quad \forall B_j \in B_k(\tau) \tag{23}$$

Proof. Consider point $B_j \in B_k(\tau)$ and denote Q_k and Q_{k+1} respectively as the intersections of the tangent line of $B_k(\tau)$ at that point with $P_{k-1}P_k$ and P_kP_{k+1} , as depicted in Figure 5. From triangle $\triangle Q_k P_k Q_{k+1}$, we have

$$\|P_k B_j\| \leq \max\{\|P_k Q_k\|, \|P_k Q_{k+1}\|\}. \tag{24}$$

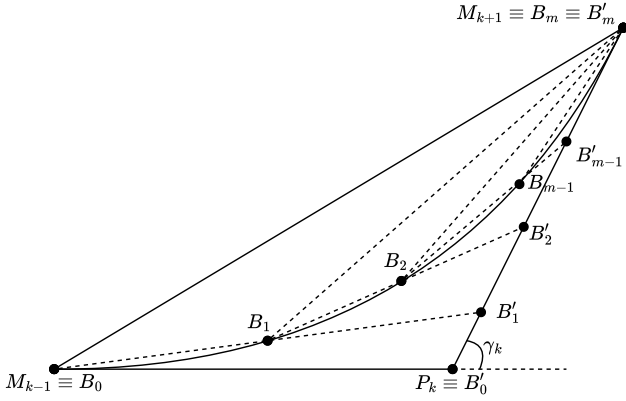


Fig. 6: Turning angles at certain points on the interpolated Bezier curve

Since $Q_k \in [M_{k-1}, P_k]$ and $Q_{k+1} \in [P_k, M_{k+1}]$, we get

$$\begin{aligned} \|P_k Q_{k+1}\| &\leq \|P_k M_{k+1}\| \\ \|P_k Q_k\| &\leq \|P_k M_{k-1}\| \end{aligned} \quad (25)$$

According to (24) and (25), and note that $\|P_k M_{k-1}\| = \|P_k M_{k+1}\| = R_k$, we have

$$\|P_k B_j\| \leq R_k \quad \forall B_j \in B_k(\tau). \quad (26)$$

□

Next, we prove that the turning angle at any point on the interpolated Bezier curve meets the dynamic constraint. Let $B = \{B_0, B_1, \dots, B_m\}$ be a set of points on $B_k(\tau)$ so that $B_0 \equiv M_{k-1}$ and $B_m \equiv M_{k+1}$, as illustrated in Figure 6. Denote $B'_0 \equiv P_k$ and B'_j as the intersection of $B_0 B_j$ and $P_k B_m$. At B_j , the turning angle of the UAV flying along the interpolated curve is $\angle B_{j+1} B_j B'_j$.

Theorem 2. *The curve $B(\tau)$ always satisfies the turning angle constraint, i.e.,*

$$\angle B_{j+1} B_j B'_j < \gamma_k \leq \gamma_{\max} \quad \forall j \in \{0, \dots, m-1\} \quad (27)$$

Proof. For all $j \in \{0, \dots, m-1\}$, consider triangle $\triangle B'_{j+1} B'_j B_j$, we have

$$\angle B'_{j+1} B_j B'_j + \angle B_j B'_{j+1} B'_j + \angle B'_{j+1} B'_j B_j = \pi. \quad (28)$$

Hence,

$$\angle B_{j+1} B_j B'_j = \angle B'_{j+1} B_j B'_j < \pi - \angle B'_{j+1} B'_j B_j. \quad (29)$$

On the other hand, consider triangle $\triangle B'_j B'_{j-1} B_{j-1}$, we have

$$\angle B'_{j+1} B'_j B_j = \angle B'_j B'_{j-1} B_{j-1} + \angle B'_j B_{j-1} B'_{j-1}. \quad (30)$$

and hence

$$\angle B'_{j+1} B'_j B_j > \angle B'_j B'_{j-1} B_{j-1}. \quad (31)$$

As a result, we get

$$\pi - \angle B'_{j+1} B'_j B_j < \pi - \angle B'_j B'_{j-1} B_{j-1}. \quad (32)$$

Applying (32) for $\forall j \in \{1, \dots, m-1\}$ gives

$$\begin{aligned} \pi - \angle B'_m B'_{m-1} B_{m-1} &< \dots < \pi - \angle B'_{j+1} B'_j B_j \\ &< \dots < \pi - \angle B'_1 B'_0 B_0 = \gamma_k. \end{aligned} \quad (33)$$

TABLE I: UAV parameters

Notation	Value	Meaning
m	1.50	Mass of the UAV (kg)
g	9.81	Gravity acceleration (m/s^2)
v_x	8.0	Velocity in the x direction (m/s)
Ω_{\max}	1000	Angular velocities of the propellers
c_t	2.9×10^{-5}	Thrust coefficient
c_f	1.1×10^{-6}	Friction coefficient

From (29) and (33), we obtain

$$\angle B_{j+1} B_j B'_j < \gamma_k. \quad (34)$$

□

Remark 1. *With Theorem 1 and Theorem 2, we prove that our path smoothing using second-order Bezier curves not only satisfies the UAV's dynamic constraint but also ensures sufficient distance from obstacles for its safe operation.*

Remark 2. *When operating at a certain forward velocity v_x , the energy consumption of the UAV is proportional to its travel distance. Since MultiRRT minimizes the path length, it reduces energy consumption.*

V. RESULTS AND DISCUSSION

To evaluate the performance of the proposed algorithm, we have conducted a number of comparisons and experiments with details as follows.

A. Scenario setup

The UAVs used in simulations and experiments are quadrotors named 3DR Solo¹, as shown in Figure 16. Their parameters are chosen as in Table I, which results in the maximum turning angle of $\gamma_{\max} = 75^\circ$. The tree-expansion distance δ is chosen as 50, and the maximum number of iterations is set to 5000.

In evaluation, four scenarios are generated with different complexity levels, as shown in Figure 7. Three metrics are used to evaluate the algorithms with definition as follows [40]–[42].

- i. *Path length:* The path length is defined as the average length of all generated paths, i.e.,

$$F_L = \frac{1}{n} \sum_{i=1}^n \sum_{j=1}^{N_i} \|P_{ij} P_{i,j+1}\|. \quad (35)$$

- ii. *Smooth score:* The smoothness score, F_S , is determined based on the angles between consecutive flight path segments, referred to as the turning angles γ , and is calculated as follows:

$$F_S = \frac{1}{n(N_i - 1)} \sum_{i=1}^n \sum_{j=2}^{N_i} \gamma_{ij}. \quad (36)$$

¹Documentation of the 3DR Solo drone is available [here](#).

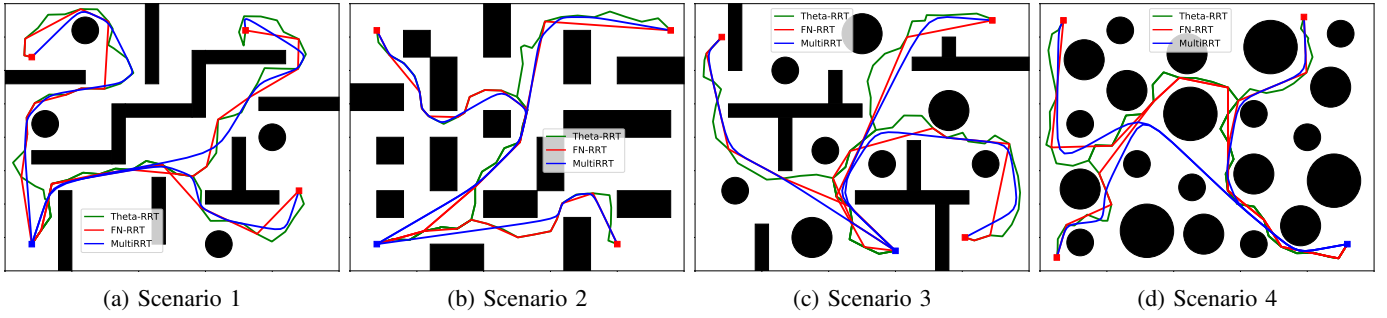


Fig. 7: The paths generated by the RRT algorithms in four scenarios

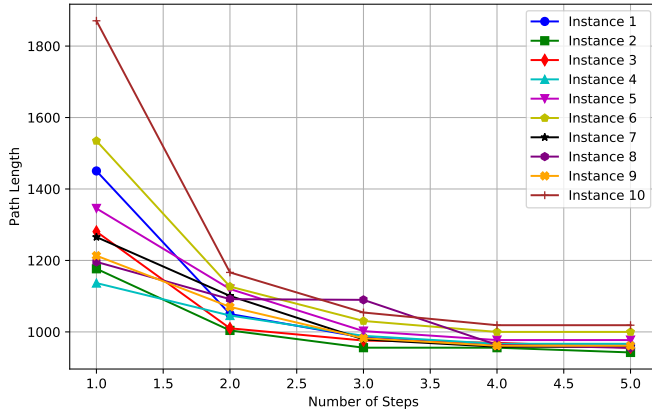


Fig. 8: Reduction in length of ten path instances during the node reduction process

The smaller the angle values, the smoother the flight paths, and vice versa. Thus, a small smooth score implies a good path as less turning operation is needed.

- iii. *Computation time:* Computation time, F_T , is the time required for the algorithm to generate paths to all the targets.

In our comparison, each algorithm is executed 10 times for each scenario. The results are then presented by box plots that include the minimum, maximum, average, and standard deviation of the obtained data.

B. Node reduction evaluation

In this section, we evaluate the effectiveness of our node reduction mechanism by comparing it with two popular RRT variants, Theta-RRT [43] and FN-RRT [44]. The Theta-RRT does not use node reduction but geometric information to optimize the path. The FN-RRT, on the other hand, employs an intensive node reduction mechanism where intermediate nodes are removed until a potential collision is detected.

The paths generated in the four scenarios are shown in Figure 7. It can be seen that all methods can create collision-free paths from the start to the target locations. However, the path length F_L of the proposed method is shortest among all scenarios. This result can be further confirmed in Figure 9, which shows the mean and variance of the path lengths in all scenarios. Thanks to our node reduction mechanism, MultiRRT obtains the smallest mean values for all four scenarios. Its

variance is also smaller than other algorithms, which implies a more stable convergence. Figure 8 illustrates the convergence process in which the path length reduces in all ten trials as redundant nodes are progressively removed at each step.

Figure 10 shows the smooth score of the algorithms. MultiRRT obtains significantly smaller values in both mean and variance than the other algorithms in all scenarios. The rationale for this is the integration of dynamic constraints and the Bezier smoothing mechanism in MultiRRT. However, they also lead to extra computation time, which is about 0.1 s compared to the fastest method, as depicted in Figure 11. This small extra calculation time does not affect the capability of MultiRRT as its overall execution time (less than 1 s) is still much faster than other approaches (see Table II) and sufficient for online replanning.

C. Comparison with other RRT variants

In this section, comparisons with other suboptimal variants of RRT, including RRT* [30], [45] and RRT*-Smart [31], are conducted to further evaluate the performance of the proposed method. As shown in Figure 12, all paths generated by the RRT variants are able to reach the targets without collision. Their path length, smoothness, and computation time in all scenarios are shown in Figures 13, 14, and 15, respectively. It can be seen that MultiRRT achieves the best score in all metrics. Especially the smooth score of the proposed method is at least three times better than the other algorithms due to the Bezier interpolation. This is an important feature of our algorithm to generate paths that the UAVs can accurately follow in practice.

D. Comparison with other approaches

To validate the performance of the proposed algorithm, we compared it with other approaches including a Voronoi-based method [46] and a particle swarm optimization (PSO)-based method [20]. The comparisons were conducted in environments with varying obstacle densities (obs/m²) of 0.16, 0.22, and 0.3. The results presented in Table II show that while PSO achieves the shortest path at a low obstacle density (0.16 obs/m²), its performance degrades in more complex scenarios. The Voronoi approach is ineffective with the worst path length scores in all scenarios. In contrast, the proposed MultiRRT algorithm shows superior performance and stability across different scenarios with nearly constant metric values even

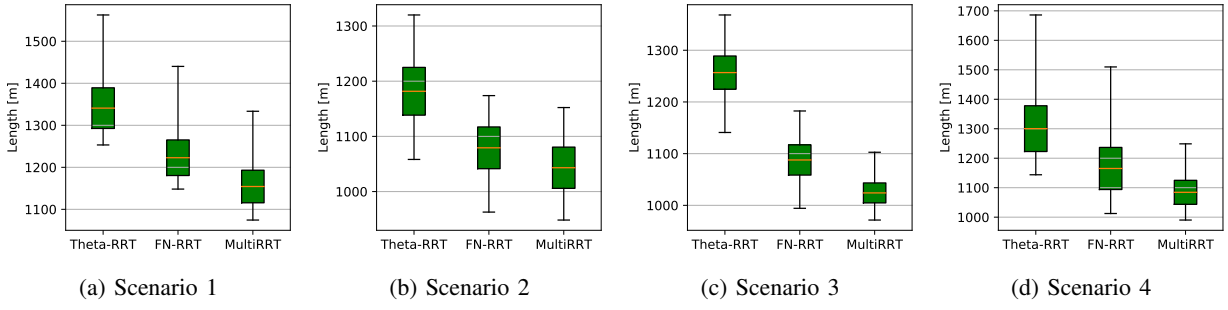
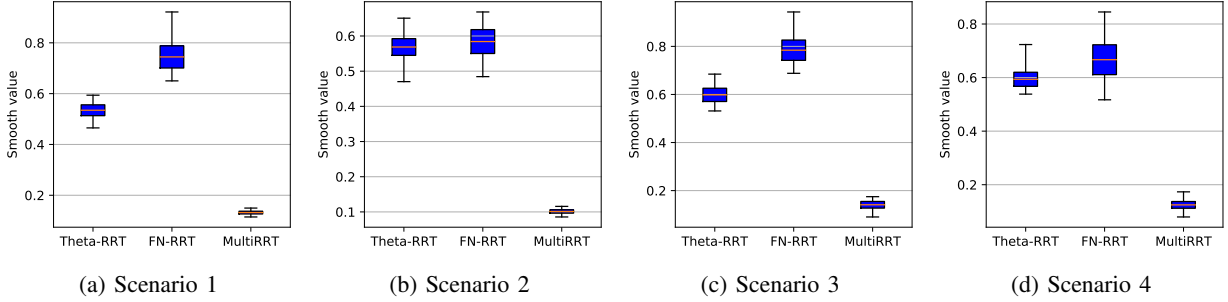
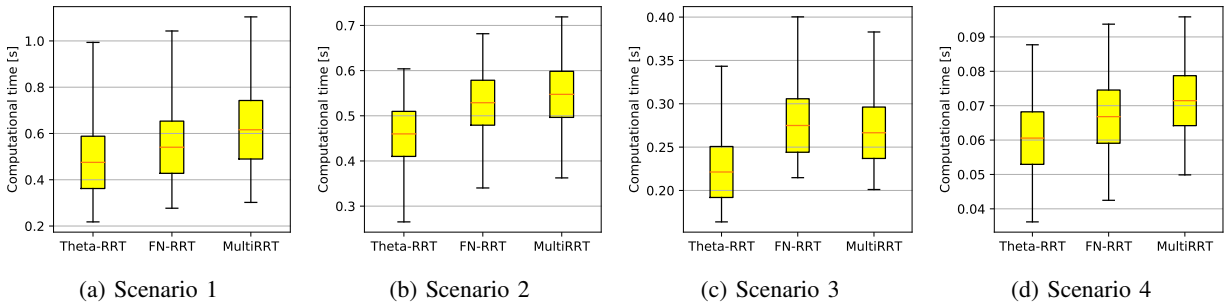
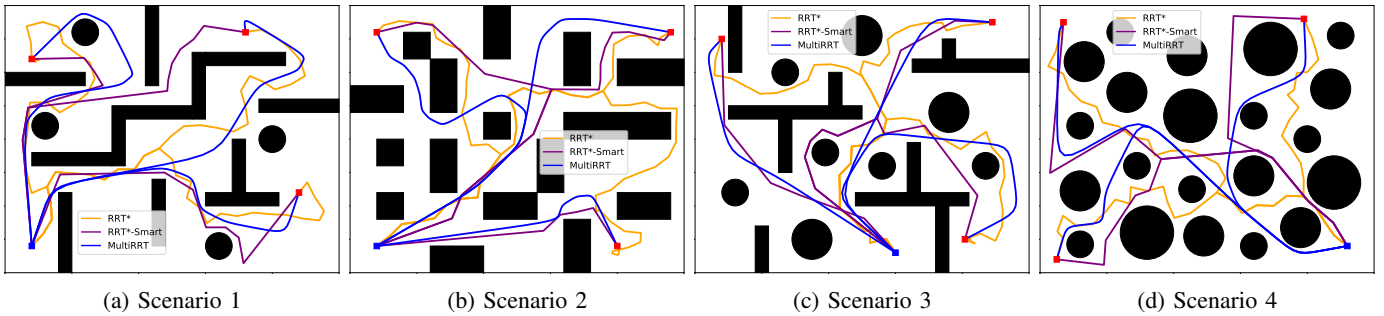
Fig. 9: The path length F_L of the comparing algorithmsFig. 10: The smooth score F_S of the comparing algorithmsFig. 11: The execution time F_T of the comparing algorithms

Fig. 12: The paths generated by the RRT algorithms

TABLE II: Comparison with other approaches

Density (obs/m ²)	F_L (m)			F_S			F_T (s)		
	PSO	Voronoi	MultiRRT	PSO	Voronoi	MultiRRT	PSO	Voronoi	MultiRRT
0.16	924.843	1355.831	937.671	0.772	0.480	0.097	106.282	55.778	0.073
0.22	1182.039	1255.206	1004.041	0.697	0.288	0.124	174.213	91.723	0.047
0.3	1213.339	1698.931	1018.017	0.976	0.199	0.117	218.718	129.561	0.056

*Bold values indicate the best scores

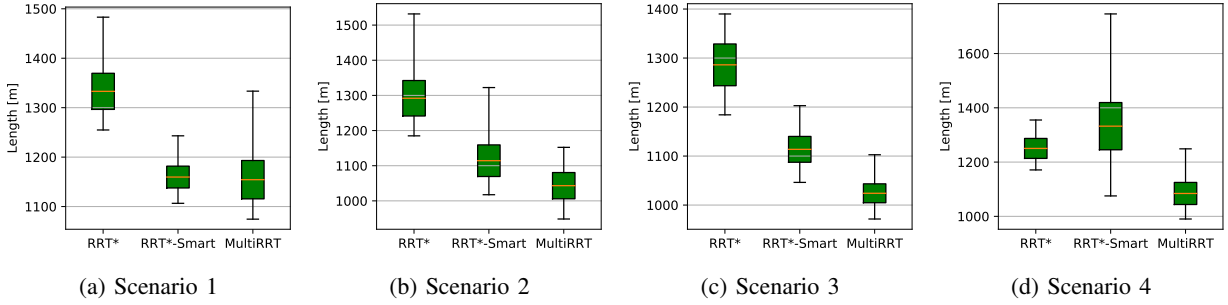
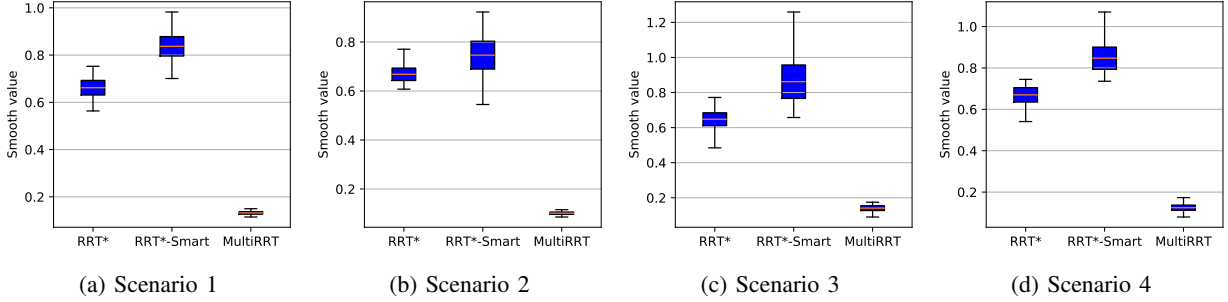
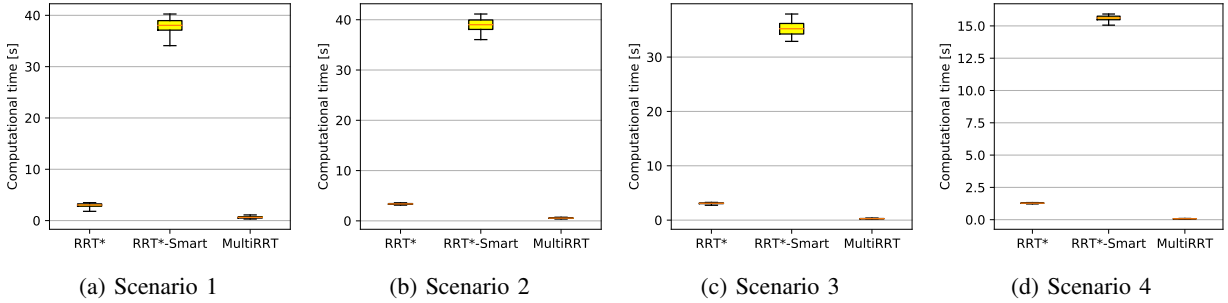
Fig. 13: The path length F_L of the RRT algorithmsFig. 14: The smooth score F_S of the RRT algorithms

Fig. 15: The execution time of the RRT algorithms

TABLE III: Scalability analysis of MultiRRT

No. of UAVs	3	5	6	8	10
F_L (m)	1138.815	1162.778	1212.089	1154.804	1137.892
F_S	0.140	0.142	0.136	0.131	0.122
F_T (s)	0.685	0.745	0.706	0.911	0.930

as obstacle density increases. Notably, its computation time is much faster than the other methods, making it suitable for real-time execution, which is essential for cooperative path planning.

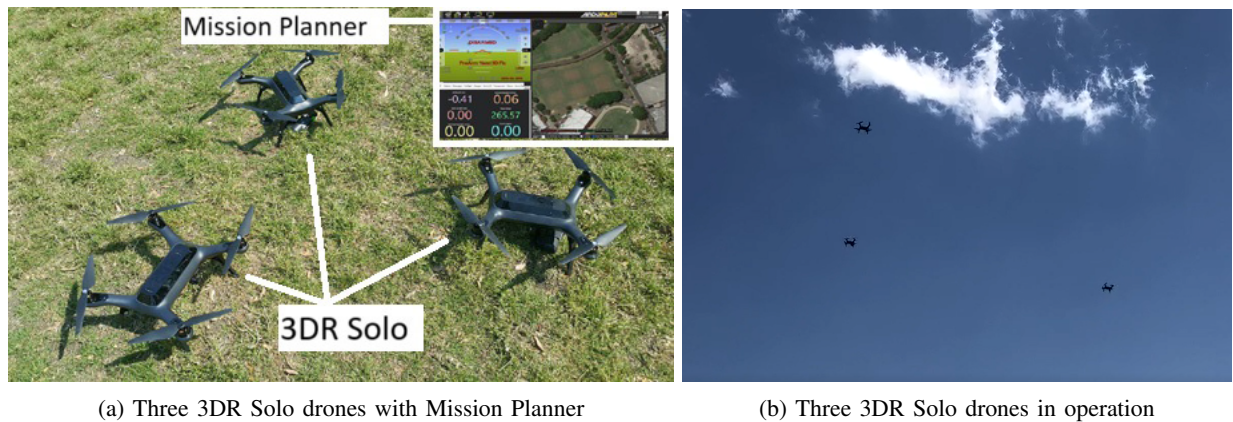
E. Scalability analysis

To analyze the scalability of the proposed method, we evaluated its performance metrics across different numbers of UAVs. As shown in Table III, the path length and smoothness scores remain stable. The extra execution time also remains minimal due to the multi-goal expansion within a single random tree in MultiRRT. These results confirm that the

proposed algorithm can be scaled to accommodate a large number of UAVs.

F. Experimental validation

To validate the applicability of MultiRRT in generating flyable paths, experiments have been conducted in an area of size $180\text{ m} \times 120\text{ m}$ within a park. The UAVs used are 3DR Solo drones that can be programmed to fly autonomously via a ground control station called Mission Planner. Figure 16a and Figure 16b respectively show the three UAVs with Mission Planner and their operation in experiments. The goal is to plan paths for the UAVs from the same starting location to three different goal locations and then upload the paths to the UAVs for automatic flight. To simulate practical scenarios, the environment is augmented with obstacles represented by red line areas shown in Figure 17. These areas represent both physical objects such as trees and bridges, and non-physical objects like no-fly zones. The start location is set at the longitude and latitude of $(-33.876289, 151.19243)$ and the goal locations are set at $(-33.875736, 151.192739)$,



(a) Three 3DR Solo drones with Mission Planner

(b) Three 3DR Solo drones in operation

Fig. 16: The drones used for experiments

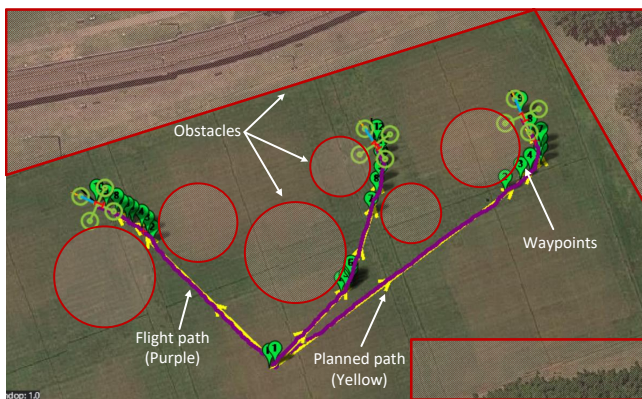


Fig. 17: Experimental result with the planned (yellow) and actual (purple) flight paths of three UAVs programmed via Mission Planner. Note that the drone symbol of Mission Planner does not reflect the actual size of the UAVs.

$(-33.875898, 151.191895)$, and $(-33.875669, 151.193161)$. The flight altitudes are set to 5 m, 10 m, and 15 m to avoid collisions among the UAVs. This information is used as input to our MultiRRT path planning program written in Python to generate paths and reference velocities for the UAVs. Each path is represented by a set of waypoints, which is then transmitted to its corresponding UAV via Mission Planner to fly automatically. During operation, if major adjustments are required such as modifying the path or reference velocity, MultiRRT can be re-executed to replan the UAVs due to its fast execution time.

Figure 17 shows the planned (yellow) and actual (purple) flight paths of the three UAVs. It can be seen that the algorithm can generate collision-free paths for all the UAVs to reach their target locations. The overlapping between the actual flight paths and the planned paths means that the generated paths meet the safety and dynamics constraints for the UAVs to follow. Especially, the UAVs show good tracking performance at curved segments. The results thus confirm the validity of the proposed algorithm for practical flights of multiple UAVs.

VI. CONCLUSION

In this paper, we have presented a novel algorithm named MultiRRT for cooperative path planning of multiple UAVs. The algorithm extends the branch expanding mechanism of RRT to reach multiple goal positions. Importantly, it integrates new features related to node reduction, dynamics constraint and Bezier interpolation to ensure the optimality, safety and feasibility of the paths generated. Unlike existing Bezier fitting techniques, our approach considers obstacle locations and dynamics limits of the UAVs to calculate relevant interpolated curves. For the first time, we prove that the interpolation meets the dynamics and safety constraints to generate feasible flight paths. Simulation, comparison, and experiment results confirm the validity and effectiveness of our approach for multiple UAV operations. Our future works will focus on integrating ad hoc communication into the system and expanding the approach to tackle real-time UAV formation for complex collaborative tasks in dynamic environments.

REFERENCES

- [1] S. Javaid, N. Saeed, Z. Qadir, H. Fahim, B. He, H. Song, and M. Bilal, "Communication and control in collaborative UAVs: Recent advances and future trends," *IEEE Transactions on Intelligent Transportation Systems*, vol. 24, no. 6, pp. 5719–5739, 2023.
- [2] W. Hu, Y. Yu, S. Liu, C. She, L. Guo, B. Vucetic, and Y. Li, "Multi-UAV coverage path planning: A distributed online cooperation method," *IEEE Transactions on Vehicular Technology*, vol. 72, no. 9, pp. 11727–11740, 2023.
- [3] H. Guo, J. Li, J. Liu, N. Tian, and N. Kato, "A survey on space-air-ground-sea integrated network security in 6g," *IEEE Communications Surveys & Tutorials*, vol. 24, no. 1, pp. 53–87, 2022.
- [4] H. T. Do, H. T. Hua, M. T. Nguyen, C. V. Nguyen, H. T. Nguyen, H. T. Nguyen, and N. T. Nguyen, "Formation control algorithms for multiple-UAVs: a comprehensive survey," *EAI Endorsed Transactions on Industrial Networks and Intelligent Systems*, vol. 8, no. 27, pp. e3–e3, 2021.
- [5] C. Xu, M. Xu, and C. Yin, "Optimized multi-UAV cooperative path planning under the complex confrontation environment," *Computer Communications*, vol. 162, p. 196–203, Oct. 2020.
- [6] L. Xu, X. Cao, W. Du, and Y. Li, "Cooperative path planning optimization for multiple UAVs with communication constraints," *Knowledge-Based Systems*, vol. 260, p. 110164, Jan. 2023.
- [7] H. Guo, Y. Wang, J. Liu, and C. Liu, "Multi-uav cooperative task offloading and resource allocation in 5g advanced and beyond," *IEEE Transactions on Wireless Communications*, vol. 23, no. 1, pp. 347–359, 2024.

- [8] H. Guo, X. Zhou, J. Wang, J. Liu, and A. Benslimane, "Intelligent task offloading and resource allocation in digital twin based aerial computing networks," *IEEE Journal on Selected Areas in Communications*, vol. 41, no. 10, pp. 3095–3110, 2023.
- [9] C. Peng, X. Huang, Y. Wu, and J. Kang, "Constrained multi-objective optimization for UAV-enabled mobile edge computing: Offloading optimization and path planning," *IEEE Wireless Communications Letters*, vol. 11, no. 4, pp. 861–865, 2022.
- [10] C. Dutriez, O. S. Oubbati, C. Gueguen, and A. Rachedi, "Energy efficiency relaying election mechanism for 5G internet of things: A deep reinforcement learning technique," in *2024 IEEE Wireless Communications and Networking Conference (WCNC)*, pp. 1–6, 2024.
- [11] J. Tang and H. Ma, "Mixed integer programming for time-optimal multi-robot coverage path planning with efficient heuristics," *IEEE Robotics and Automation Letters*, vol. 8, no. 10, pp. 6491–6498, 2023.
- [12] D. Ioan, I. Prodan, S. Olaru, F. Stoican, and S.-I. Niculescu, "Mixed-integer programming in motion planning," *Annual Reviews in Control*, vol. 51, p. 65–87, 2021.
- [13] A. Britzelmeier, A. De Marchi, and R. Richter, "Dynamic and nonlinear programming for trajectory planning," *IEEE Control Systems Letters*, vol. 7, pp. 2569–2574, 2023.
- [14] B. A. Asfora, J. Banfi, and M. Campbell, "Mixed-integer linear programming models for multi-robot non-adversarial search," *IEEE Robotics and Automation Letters*, vol. 5, no. 4, pp. 6805–6812, 2020.
- [15] D. Bauso, L. Giarre, and R. Pesenti, "Multiple UAV cooperative path planning via neuro-dynamic programming," in *2004 43rd IEEE Conference on Decision and Control (CDC) (IEEE Cat. No.04CH37601)*, vol. 1, pp. 1087–1092 Vol.1, 2004.
- [16] Y. Cao, W. Wei, Y. Bai, and H. Qiao, "Multi-base multi-UAV cooperative reconnaissance path planning with genetic algorithm," *Cluster Computing*, vol. 22, pp. 5175–5184, 2019.
- [17] Z. A. Ali, H. Zhangang, and D. Zhengru, "Path planning of multiple UAVs using MMACO and DE algorithm in dynamic environment," *Measurement and Control*, vol. 56, no. 3-4, pp. 459–469, 2023.
- [18] P. Yao, H. Wang, and H. Ji, "Multi-UAVs tracking target in urban environment by model predictive control and improved grey wolf optimizer," *Aerospace Science and Technology*, vol. 55, p. 131–143, Aug. 2016.
- [19] D. N. Bui, T. N. Duong, and M. D. Phung, "Ant colony optimization for cooperative inspection path planning using multiple unmanned aerial vehicles," in *2024 IEEE/SICE International Symposium on System Integration (SII)*, pp. 675–680, 2024.
- [20] P. Das and P. Jena, "Multi-robot path planning using improved particle swarm optimization algorithm through novel evolutionary operators," *Applied Soft Computing*, vol. 92, p. 106312, July 2020.
- [21] H. M. Jayaweera and S. Hanoun, "A dynamic artificial potential field (d-apf) UAV path planning technique for following ground moving targets," *IEEE Access*, vol. 8, pp. 192760–192776, 2020.
- [22] H. Li, W. Liu, C. Yang, W. Wang, T. Qie, and C. Xiang, "An optimization-based path planning approach for autonomous vehicles using the dynefwa-artificial potential field," *IEEE Transactions on Intelligent Vehicles*, vol. 7, no. 2, pp. 263–272, 2022.
- [23] Z. Pan, C. Zhang, Y. Xia, H. Xiong, and X. Shao, "An improved artificial potential field method for path planning and formation control of the multi-UAV systems," *IEEE Transactions on Circuits and Systems II: Express Briefs*, vol. 69, no. 3, pp. 1129–1133, 2022.
- [24] E. Wu, Y. Sun, J. Huang, C. Zhang, and Z. Li, "Multi UAV cluster control method based on virtual core in improved artificial potential field," *IEEE Access*, vol. 8, pp. 131647–131661, 2020.
- [25] T. Dang, M. Tranzatto, S. Khattak, F. Mascarich, K. Alexis, and M. Hutter, "Graph-based subterranean exploration path planning using aerial and legged robots," *Journal of Field Robotics*, vol. 37, no. 8, pp. 1363–1388, 2020.
- [26] M. Baumann, S. Léonard, E. A. Croft, and J. J. Little, "Path planning for improved visibility using a probabilistic road map," *IEEE Transactions on Robotics*, vol. 26, no. 1, pp. 195–200, 2010.
- [27] S. M. LaValle and J. James J. Kuffner, "Randomized kinodynamic planning," *The International Journal of Robotics Research*, vol. 20, no. 5, pp. 378–400, 2001.
- [28] F. Yan, Y.-S. Liu, and J.-Z. Xiao, "Path planning in complex 3d environments using a probabilistic roadmap method," *International Journal of Automation and computing*, vol. 10, pp. 525–533, 2013.
- [29] M. Kothari and I. Postlethwaite, "A probabilistically robust path planning algorithm for UAVs using rapidly-exploring random trees," *Journal of Intelligent & Robotic Systems*, vol. 71, pp. 231–253, 2013.
- [30] S. Karaman and E. Frazzoli, "Sampling-based algorithms for optimal motion planning," *The International Journal of Robotics Research*, vol. 30, p. 846–894, June 2011.
- [31] J. Nasir, F. Islam, U. Malik, Y. Ayaz, O. Hasan, M. Khan, and M. S. Muhammad, "RRT*-SMART: A rapid convergence implementation of RRT*," *International Journal of Advanced Robotic Systems*, vol. 10, p. 299, Jan. 2013.
- [32] O. S. Oubbati, H. Badis, A. Rachedi, A. Lakas, and P. Lorenz, "Multi-UAV assisted network coverage optimization for rescue operations using reinforcement learning," in *2023 IEEE 20th Consumer Communications & Networking Conference (CCNC)*, pp. 1003–1008, 2023.
- [33] A. I. Ameur, O. S. Oubbati, A. Lakas, A. Rachedi, and M. B. Yagoubi, "Efficient vehicular data sharing using aerial P2P backbone," *IEEE Transactions on Intelligent Vehicles*, pp. 1–14, 2024.
- [34] J. Luo, Z. Wang, M. Xia, L. Wu, Y. Tian, and Y. Chen, "Path planning for UAV communication networks: Related technologies, solutions, and opportunities," *ACM Computing Surveys*, vol. 55, no. 9, pp. 1–37, 2023.
- [35] M. T. Nguyen, C. V. Nguyen, H. T. Do, H. T. Hua, T. A. Tran, A. D. Nguyen, G. Ala, and F. Viola, "UAV-assisted data collection in wireless sensor networks: A comprehensive survey," *Electronics*, vol. 10, no. 21, 2021.
- [36] X. C. Ding, A. R. Rahmani, and M. Egerstedt, "Multi-UAV convoy protection: An optimal approach to path planning and coordination," *IEEE Transactions on Robotics*, vol. 26, no. 2, pp. 256–268, 2010.
- [37] S. G. Manyam, S. Rathinam, D. Casbeer, and E. Garcia, "Tightly bounding the shortest dubins paths through a sequence of points," *Journal of Intelligent & Robotic Systems*, vol. 88, no. 2, pp. 495–511, 2017.
- [38] W. Yao, N. Qi, J. Zhao, and N. Wan, "Bounded curvature path planning with expected length for dubins vehicle entering target manifold," *Robotics and Autonomous Systems*, vol. 97, pp. 217–229, 2017.
- [39] C. Wang, B. Song, P. Huang, and C. Tang, "Trajectory tracking control for quadrotor robot subject to payload variation and wind gust disturbance," *Journal of Intelligent & Robotic Systems*, vol. 83, pp. 315–333, Aug 2016.
- [40] M. D. Phung and Q. P. Ha, "Safety-enhanced UAV path planning with spherical vector-based particle swarm optimization," *Applied Soft Computing*, vol. 107, p. 107376, Aug. 2021.
- [41] A. Puente-Castro, D. Rivero, A. Pazos, and E. Fernandez-Blanco, "UAV swarm path planning with reinforcement learning for field prospecting," *Applied Intelligence*, vol. 52, p. 14101–14118, Mar. 2022.
- [42] X. Wu, L. Xu, R. Zhen, and X. Wu, "Bi-directional adaptive A* algorithm toward optimal path planning for large-scale UAV under multi-constraints," *IEEE Access*, vol. 8, pp. 85431–85440, 2020.
- [43] L. Palmieri, S. Koenig, and K. O. Arras, "RRT-based nonholonomic motion planning using any-angle path biasing," in *2016 IEEE International Conference on Robotics and Automation (ICRA)*, pp. 2775–2781, 2016.
- [44] J. Qi, Q. Yuan, C. Wang, X. Du, F. Du, and A. Ren, "Path planning and collision avoidance based on the RRT*FN framework for a robotic manipulator in various scenarios," *Complex & Intelligent Systems*, vol. 9, p. 7475–7494, July 2023.
- [45] X. Wang, J. Gao, X. Zhou, and X. Gu, "Path planning for the gantry welding robot system based on improved RRT*," *Robotics and Computer-Integrated Manufacturing*, vol. 85, p. 102643, Feb. 2024.
- [46] S.-K. Huang, W.-J. Wang, and C.-H. Sun, "A new multirobot path planning with priority order based on the generalized voronoi diagram," *IEEE Access*, vol. 10, pp. 56564–56577, 2022.



Thu Hang Khuat received her B.Eng. degree in Robotics Engineering from VNU University of Engineering and Technology in 2023. She is currently pursuing an M.Sc. degree in Electronics Engineering at the same institution. Her research interests include robotics, unmanned aerial vehicles (UAVs), path planning, and swarm optimization.



Duy Nam Bui received his B.Eng. degree in Robotics Engineering and M.Sc. degree in Electronics Engineering from VNU University of Engineering and Technology, Hanoi, Vietnam, in 2022 and 2024, respectively. His current research interests include formation control and cooperative path planning of multi-robot systems, as well as learning and optimization.



Manh Duong Phung received his Ph.D. from Vietnam National University, Hanoi, in 2015 and completed a postdoctoral fellowship at the University of Technology Sydney in 2017. He is currently a Senior Lecturer at Fulbright University Vietnam. His research interests include unmanned aerial vehicles, autonomous robots, and swarm intelligence. He has served on the organizing committees of various international conferences and as a reviewer for reputable journals published by IEEE, Elsevier, and Springer. He is the recipient of several research awards, including the Endeavour Research Fellowship from the Australian Government and the Best Paper Award at the Australasian Conference on Robotics and Automation.



Hoa T. T. Nguyen received her B.S., M.S. degrees in Control Engineering and Automation from Thai Nguyen University of Technology, Viet Nam in 2013 and 2017, respectively. M.S. Hoa T. Nguyen is currently working as a lecturer and researcher at faculty of electronics engineering, Thai Nguyen University of Technology (TNUT), Vietnam, and also a member of Advanced Wireless Communication Networks (AWCN) Lab. She has interest and expertise in a variety of research topics in Automation, Control Systems, UAV networks, Formation Control,

Adaptive Control, and Intelligent Systems.



Mien L. Trinh obtained his Ph.D. from the Russian University of Transport in 2012. He is currently an Associate Professor, Head of Laboratory, Deputy Head of the Department of Cybernetics, and Vice Dean of the Faculty of Electrical and Electronic Engineering at the University of Transport and Communications, Vietnam. His research interests and expertise span a variety of topics in control and automation of machines and production lines, with a particular focus on intelligent control for electric vehicles, electric trains, robotics, and UAV networks.



Minh T. Nguyen received his B.S., M.S., and Ph.D. degrees in Electrical Engineering from Hanoi University of Communication and Transport, Vietnam in 2001; Military Technical Academy, Hanoi, Vietnam in 2007; and Oklahoma State University, Stillwater, OK, USA in 2015, respectively. He is currently the Director of the Human Resource Training and Development Center (HDC) at Thai Nguyen University (TNU), a teaching and research professor at Thai Nguyen University of Technology (TNUT), Vietnam, and the Director of the Advanced Wireless

Communication Networks (AWCN) Lab. His research interests and expertise span a wide range of topics in communications, networking, and signal processing, with a particular focus on compressive sensing, wireless/mobile sensor networks, robotics, and UAV networks. He serves as a technical reviewer for several prestigious journals and international conferences. He is also an editor for *Wireless Communications and Mobile Computing*, *EAI Endorsed Transactions on Industrial Networks and Intelligent Systems*, and serves as Editor-in-Chief of *ICSES Transactions on Computer Networks and Communications*.